Advances in high-resolution imaging – techniques for three-dimensional imaging of cellular structures

Diane S. Lidke[1] and Keith A. Lidke[2,*]

[1]Department of Pathology and Cancer Research and Treatment Center, University of New Mexico, Albuquerque, NM 87131, USA
[2]Department of Physics, University of New Mexico, Albuquerque, NM 87131, USA
*Author for correspondence (klidke@unm.edu)

Journal of Cell Science 125, 2571–2580

doi: 10.1242/jcs.090027

Summary

A fundamental goal in biology is to determine how cellular organization is coupled to function. To achieve this goal, a better understanding of organelle composition and structure is needed. Although visualization of cellular organelles using fluorescence or electron microscopy (EM) has become a common tool for the cell biologist, recent advances are providing a clearer picture of the cell than ever before. In particular, advanced light-microscopy techniques are achieving resolutions below the diffraction limit and EM tomography provides high-resolution three-dimensional (3D) images of cellular structures. The ability to perform both fluorescence and electron microscopy on the same sample (correlative light and electron microscopy, CLEM) makes it possible to identify where a fluorescently labeled protein is located with respect to organelle structures visualized by EM. Here, we review the current state of the art in 3D biological imaging techniques with a focus on recent advances in electron microscopy and fluorescence super-resolution techniques.

Key words: Correlative light and electron microscopy, Electron microscopy, Super resolution

Introduction

It has been more than 50 years since the details of cellular structure were first observed with an electron microscope (Porter et al., 1945). Today, electron microscopy (EM) still provides the highest resolution detail of cellular ultrastructure. Although EM sample preparation can potentially alter cellular structure, advances in preservation techniques, such as high-pressure freezing, make it possible to retain structures for a nearly native view of cellular components (Koster and Klumperman, 2003). A better understanding of the molecular make-up of a cell can be obtained through immuno-EM (i.e. labeling of proteins of interest with antibodies), which reveals the localization of specific proteins with respect to cellular compartments (Box 1). However, immuno-EM does have its limitations: penetration of large gold particles into the sample can be inconsistent, only one or two protein targets can be distinguished and the samples must be fixed.

By specifically targeting cellular components with fluorescent labels, fluorescence microscopy overcomes several of the disadvantages of immuno-EM. In particular, multi-color imaging (of two or more spectrally distinct labels) is relatively easy to achieve and small organic dyes more readily penetrate cells and tissue. Furthermore, the introduction of genetically expressible tags means direct labeling of targets can be achieved without relying on antibodies (Box 1). Fluorescence microscopy also allows for live-cell imaging. Despite these advantages, conventional fluorescence microscopy is limited in resolution (~250 nm laterally and 500 nm axially) compared with EM. However, recent advances in fluorescence microscopy techniques are achieving much higher spatial resolution and are beginning to fill the gap between EM and fluorescence microscopy.

Although transmission electron microscopy (TEM) and confocal microscopy are standard tools for many cell biologists, this Commentary will highlight technologies that advance 3D cellular imaging. This includes recent demonstrations of EM serial sectioning, biological applications of focused ion-beam scanning electron microscopy (FIB-SEM) and discussion of light-microscopy techniques that provide improved resolution over the confocal microscope. At the end, we briefly discuss how these two disparate microscopies have been combined to determine the location of fluorescently labeled structures within the landscape of an electron micrograph. Many excellent reviews have been written that provide in depth detail on each of these techniques. We focus here on examples of where 3D imaging has provided new biological insight, as well as pointing out the advantages and limitations of each technique.

Building a 3D image with electron tomography

TEM images are acquired by creating sections of the sample that are thin enough for electrons to pass through. Although TEM provides nanometer lateral spatial resolution, any depth information is lost as structures overlapping in the *z*-dimension are projected into the same plane. Typically, sections are made very thin (50–100 nm) to reduce structure overlap. In EM tomography (EMT), a series of TEM images from the same sample is collected though a range of angles, from which a 3D image can be reconstructed (reviewed by Chen et al., 2008). This allows for interrogation of much thicker sections, on the order of microns. The ability to create 3D representations of cellular ultrastructure has provided new insights into biological processes that could not be gleaned from two dimensions alone.

A classic example comes from the model of mitochondria structure. Initial EM images of mitochondria lead to the model of mitochondrial cristae resulting from folds of the continuous inner membrane (Palade, 1952). More than 40 years later, the first EM tomograms of isolated rat liver mitochondria showed that the cristae are actually comprised of a heterogeneous tubular network

Box 1. Labeling of cellular targets

Electron microscopy

Immunogold labeling

Gold-conjugated antibodies are used to target specific proteins. Distinct sizes of gold particles can be used to identify different protein species on the same sample (Wilson et al., 2000; Murk et al., 2004). Owing to a lack of uniformity in particle size distribution and the fact that larger gold particles (>10 nm) show reduced labeling efficiency, labeling is typically limited to two sizes.

Osmophillic precipitates

Excitation of a fluorophore produces singlet oxygen that oxidizes diaminobenzidine (DAB) and generates an osmophylic precipitate around the labeled protein. Typically, fluorescently labeled antibodies are used to target the proteins. Recently, a new fluorescent protein that is also a singlet oxygen generator has been produced (Shu et al., 2011).

Fluorescence microscopy

Photoswitchable dyes

Organic dyes that can be reversibly photoswitched between fluorescent and dark states. They are targeted to a protein by antibody labeling or a genetically encoded peptide. Some dyes have special buffer requirements (Rust et al., 2006; Heilemann et al., 2008).

Genetically encoded tags

Fluorescent proteins. The family of fluorescent proteins provides a range of excitation and emission wavelengths, as well as photoactivatable and photoswitchable variants (Patterson et al., 2010).

Peptides. Amino acid sequences that provide a specific binding site for exogenously added dyes (Regoes and Hehl, 2005; Jacquier et al., 2006; Szent-Gyorgyi et al., 2008).

Quantum dots

Semiconducting nanocrystals, or quantum dots, can be conjugated to antibodies or ligands. Although their larger size (>10 nm) can be a disadvantage, quantum dot brightness and photostability provide clear advantages over organic dyes. quantum dot blinking can be used for super-resolution (Dertinger et al., 2009) and the electron dense core can be imaged in EM (Giepmans et al., 2005).

(Mannella et al., 1994; Mannella et al., 1997). High resolution EMT has also revealed physical interaction between mitochondria and the endoplasmatic reticulum (ER), suggesting a functional interplay between these two compartments. Rizzuto et al. have shown that, owing to their proximity, release of Ca^{2+} from the ER results in exposure of mitochondria to higher levels of Ca^{2+} than that distributed in the cytosol (Rizzuto et al., 1998). To further explore the effect of cellular geometry on signaling, Mazel et al. have built a 3D tomographic reconstruction of a single slice through a rat basophilic leukemia cell and incorporated the 3D cellular geometry into stochastic modeling of inositol-trisphosphate-mediated Ca^{2+} responses (Mazel et al., 2009). Their model predicts that the proximity of the ER to the plasma membrane or mitochondria influences inositol trisphosphate receptor transport. These results demonstrate the importance of measuring spatial organization and incorporating that knowledge into our understanding of function.

To gain extended information regarding sample depth, tomograms from individual serial sections can be aligned to create a larger continuous volume. Using serial-section EMT, West et al. have examined the 3D-structure of the ER in budding yeast cells with ~4-nm resolution (West et al., 2011). In this elegant work, the authors were able to distinguish three distinct ER structures: cisternae, tubular and plasma-membrane-associated ER (Fig. 1). On the basis of previous two-dimensional (2D) electron micrographs, it was thought that only tubular ER traversed the cytoplasm. However, the 3D volume projections generated by EMT demonstrate that some of the structures thought to be tubular ER are in fact central cisternal ER (West et al., 2011).

Although they provide exquisite structural detail, reconstruction from serial sections is incredibly time consuming and labor intensive; data collection and analysis can take days to weeks per cell (Noske et al., 2008). Individual sections can be reconstructed from tomographic data with a resolution of ~4 nm. However, material missing between sections owing to physical cutting of the sample can lead to artifacts. It is also important to note that the use of fiducial markers for proper alignment between sections is crucial to 3D reconstruction. FIB-SEM (also called ion abrasion SEM), however, allows for more precise sectioning by ablation of material from the sample in between imaging scans. FIB-SEM uses an electron beam to capture the SEM image of the sample surface, followed by an ion beam to remove a layer of material (15–50 nm) that then exposes a new section for imaging (Bushby et al., 2011). The series of SEM images are then merged to form a 3D reconstruction of the sample. With this technique, a resolution of ~20–40 nm is achieved for thick 3D samples without the need to manually generate serial sections. Best results for imaging cellular architecture have used plastic embedded cells or tissue (Heymann et al., 2009; Lešer et al., 2009). FIB-SEM does have some disadvantages, such as the loss of the section after milling,

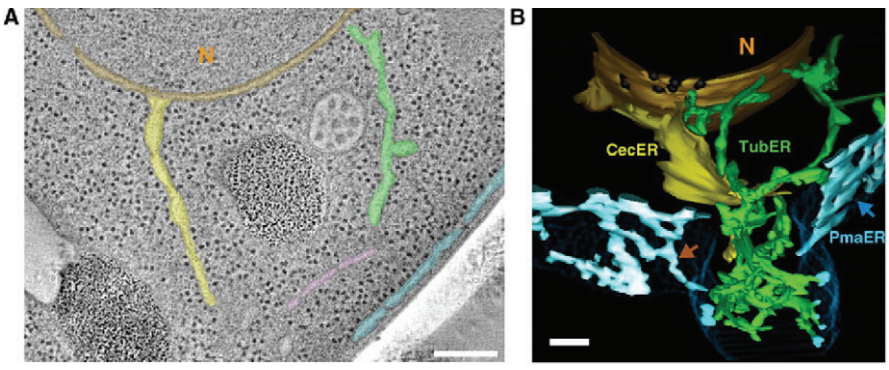

Fig. 1. 3D EM tomography. To examine ER structure at high resolution, West et al. generated tomograms from 200-nm thick sections of yeast cells (West et al., 2011). (**A**) A two-dimensional EMT image shows the nuclear envelope (N, orange), Golgi (pink) and ER structures. Scale bar: 200 nm. (**B**) The reconstructed 3D model reveals the cisternae (yellow, CecER), tubular (green, TubER) ER and plasma-membrane-associated ER (blue, PmaER). Scale bar: 100 nm. Image reproduced from West et al., 2011 (West et al., 2011).

so that repeated imaging cannot be performed, and the risk of damaging the sample surface with the ion beam.

One example of the application of FIB-SEM to biology is in studying conditions affecting mitochondria, such as methylmalonic acidemia (MMA), a metabolic disease that alters mitochondrial function. 2D TEM comparing normal and diseased mice has shown that MMA causes enlarged mitochondria, or megamitochondria (Chandler et al., 2009). However, such megamitochondria are only observed in tissue from older mice. Murphy et al. used FIB-SEM to quantify differences in mitochondria morphology in liver tissue of 4-day-old MMA mice, before megamitochondria occurs (Murphy et al., 2010). They found that although there are no striking differences in mitochondria volume or surface area between control and disease mice, the surface-area-to-volume ratio is significantly larger with a more heterogeneous size distribution in MMA mice. This can be attributed to the fact that diseased mitochondria are found to be more convoluted than the control mitochondria, a result that could not be observed from 2D TEM.

Although 3D imaging with EM continues to improve further, serial-section EMT approaches are relatively well-established techniques that have already provided important insights into biological problems. Typically, cell biologists have access to these technologies through local core facilities or national centers (for example, the National Center for Microscopy and Imaging Research at University California, San Diego, La Jolla, CA). The use of FIB-SEM requires a specialized instrument but is becoming more common in core facilities.

3D fluorescence imaging beyond the confocal microscope

Fluorescence microscopy greatly improves upon the molecular specificity of immuno-EM and can be used for live-cell imaging. The conventional standard for 3D fluorescence imaging is the laser scanning confocal microscope that is ubiquitous in microscopy core facilities. However, many organelles and cellular components have (possibly functionally relevant) structures that cannot be resolved with the confocal microscope. Here, we give an overview of several techniques that are able to image throughout a cell with a practical resolution that is greater than that of a confocal microscope, including 4pi, structured illumination (SIM), plane illumination, single-molecule-localization-based super-resolution (SML-SR) and stimulated emission depletion (STED) microscopy. We will not describe in great detail the technologies behind these various imaging techniques, but details can be found in many recent review articles (Hell, 2007; Huang et al., 2009; Schermelleh et al., 2010; Toomre and Bewersdorf, 2010; Galbraith and Galbraith, 2011). Instead, we give a brief summary of the working principle and provide examples of how these techniques have been applied in 3D intracellular imaging.

Although all of the techniques below provide higher resolution than confocal microscopy, they vary widely with regard to resolution improvement, experimental complexity, cost, multi-color capability and the applicability to live-cell imaging. Some of the techniques have only been developed in the past few years and are restricted to a handful of laboratories, whereas many of the techniques can be found in commercial products. In Box 2, we summarize the primary practical aspects that differ from conventional confocal microscopy and require either extra effort or specialized knowledge by the investigator.

4pi microscopy

4pi microscopy is a point-scanning technique that uses two opposing objectives positioned in the same focal plane in the sample (Hell and Stelzer, 1992). The technique takes its name from the fact that two opposing objective lenses with high numerical aperture approximate an ideal 4pi steradian aperture. The two lenses work together coherently to provide an increased aperture for the excitation light, the fluorescence emission or both (Fig. 2A). The increased aperture results in a diffraction-limited axial resolution of ~100 nm (Bewersdorf et al., 2006). Although now discontinued, the 4pi microscope sold by Leica Microsystems (Leica TCS 4PI) was the first commercially available fluorescence super-resolution microscope. This technique has provided some of the first demonstrations of biological studies that made use of fluorescence super-resolution. Below we highlight a few examples.

Bewersdorf et al. have used 4pi microscopy to determine the effects of ionizing radiation (IR) on the DNA repair protein H2AX (Bewersdorf et al., 2006). They fixed HeLa cells at various time points after IR exposure and used antibody labeling to compare phosphorylated (γ-H2AX) and unphosphorylated H2AX. Two-color labeling was achieved with organic-dye-conjugated secondary anitbodies (Alexa Fluor 488 and either Alexa Fluor 647 or Rhodamine Red-X). The resulting 100-nm axial resolution showed that H2AX and γ-H2AX exist as discrete clusters that are dispersed throughout the 3D volume of the nucleus. IR exposure led to an increase in the size of the γ-H2AX clusters but not of H2AX (Bewersdorf et al., 2006). These results suggest that DNA repair mechanisms proceed through a localized expansion of chromatin structure near double-strand breaks.

Dlasková et al. have used 4pi microscopy to image the complex and dense 3D mitochondrial network and compare the mitochondrial structure in cells from normal and diabetic rats. (Dlasková et al., 2010) (Fig. 2A). Here, the mitochondria were labeled using a green fluorescent protein (GFP) variant fused to a peptide that was targeted to the mitochondria. The enhanced axial resolution afforded by 4pi revealed that the tubular network of mitochondria in primary β-cells from diabetic Goto Kakizaki rats had increases in mitochondria fragmentation as compared with cells from control rats.

Structured illumination microscopy

In SIM, a series of periodic patterns are used to excite the sample. The observed Moiré emission patterns that are generated by the illumination structure and the sample contains information about the sample that can be used to generate a high-resolution image (Gustafsson et al., 2008). A series of images are collected while scanning the illumination pattern across the sample and used to reconstruct an image with a lateral resolution improved by about a factor of two compared with that of confocal microscopy. Gustafsson et al. have shown that the technique is capable of improving resolution in both lateral and axial dimensions by imaging the actin cytoskeleton throughout fixed HeLa cells using a Rhodamine–phalloidin label (Gustafsson et al., 2008). They report ~100-nm lateral and 300-nm axial resolution. In another study, Schermelleh et al. use this approach for simultaneous, 3D, multicolor imaging of DNA, nuclear lamina and nuclear pore complex (NPC) epitopes that were immunofluorescence-labeled in C2C12 cells (Schermelleh et al., 2008). The resolution of the SIM images revealed differences in the localization of two NPC epitopes with respect to the nuclear membrane (Fig. 2B). By

Box 2. Practical considerations for 3D fluorescence microscopy

Labeling

Imaging continuous structures with higher resolution requires higher labeling density. For 3D structures, this scales inversely as the resolvable imaging volume. For example, an isotropic resolution enhancement of two requires eight times the labeling density, whereas an isotropic resolution of 100 nm requires ~30 times the labeling density that would be acceptable in a confocal microscope.

Difficulty of using existing instrumentation as compared with confocal microscopy

The table below illustrates the difficulty of using the various techniques compared with using confocal microscopy. Green shading indicates a similar level of difficulty, yellow shading indicates moderately increased difficulty, and red shading indicates substantially increased difficulty. The number refers to the specific points outlined below the table.

Technique	Instrument preparation	Sample preparation	Multi-color	Post processing	Live-cell imaging
4pi	1	2, 3	5	8	12
SIM				9	13
Plane illumination		3		10	
SML-SR		4	6	11	14
STED			7		12

(1) Requires careful alignment of the two objectives and phase matching of the interferometer arms.
(2) Requires matching the index of refraction of the sample to the objective immersion medium.
(3) Samples must be mounted between two coverslips, preventing easy access to the sample.
(4) Photo-switching of organic dyes typically requires de-oxygenated buffers.
(5) Implementation with coherent excitation only requires fluorophores that can be excited simultaneously with the same two-photon excitation wavelength. Implementation that uses coherent collection of emission requires chromatic aberration correction in the emission pathway and mandates serial imaging with adjustments between imaging the different label species.
(6) When using green-to-red photo-switching proteins, serial imaging of the green-to-red and then the green protein is required (Shroff et al., 2007). Red photoactivatable proteins canbe used simultaneously with green photoactivatable or photoswitchable proteins (Subach et al., 2009) but are not as bright as green-to-red switchable proteins (Patterson et al., 2010). The blinking statistics of organic dyes varies widely and is related to the specific chemistry of the dye, buffer conditions, excitation wavelength and excitation power (Heilemann et al., 2008; Dempsey et al., 2009).
(7) The dyes must be carefully selected and matched to the available excitation and depletion wavelengths.
(8) Requires linear or non-linear deconvolution to remove axial side lobes. Users must be aware of potential artifacts in image reconstruction.
(9) Relies upon post-processing to generate images from the data.Users must be aware of potential artifacts in image reconstruction.
(10) Light-sheet approaches that employ structured illumination require additional post-processing.
(11) Requires algorithms for identification and localization of individual fluorophores. Users must be aware of potential artifacts in image reconstruction.
(12) Implemented as a point scanning technique, the collection time required scales proportionally with the volume and inversely with the sampling required for higher resolutions giving a trade-off between imaging volume, resolution, and collection time.
(13) Requires the collection of several images per *x-y* plane, but collection time does not scale with lateral size.
(14) Requires hundreds to thousands of *x-y* images for each ~1-μm-deep focal plane giving a trade off of sampling density with collection time.

introducing a dual objective format, Shao et al. further improved the axial resolution of SIM and were able to image the microtubule network of HeLa cells with ~100-nm isotropic resolution (Shao et al., 2008). 3D SIM uses standard labeling protocols, is easily implemented in multicolor imaging and offers a resolution improvement of a factor of two that might be sufficient for many biological studies.

Plane illumination microscopy

Extended time series imaging in three dimensions using confocal microscopy has the problem that the out-of-focus planes also are illuminated, causing photobleaching of the fluorophores and photo-toxic effects. This can be detrimental for imaging of fixed cells but certainly hampers time series imaging of live cells. Multi-photon excitation can reduce this effect, but the resolution is not improved over confocal microscopy. Techniques using two perpendicular objectives, one for imaging and a second for generating an excitation light sheet in the focal plane of the sample, have been developed for extended time series imaging in multicellular organisms (Keller et al., 2008; Huisken and Stainier, 2009). Their benefit derives from the fact that only the in-focus plane is illuminated, greatly extending the number of usable fluorophore imaging cycles and reducing the background fluorescence. This technique was originally developed for imaging of larger multicellular organisms. However, the light sheets used could only be made ~1 μm in height and thus axial resolution is not improved.

Recently, Planchon et al. have demonstrated a modified version of the light-sheet approach that they optimized for single-cell imaging. In order to reduce the thickness of the light sheet, they used a special mode of light called a Bessel beam to produce a long thin pencil of light that is scanned through the focal plane (Planchon et al., 2011) (Fig. 2C). However, the Bessel beams consist of both a central beam of light and concentric rings around this beam. The brighter, central beam is positioned in the focal plane of the imaging objective, yet the outer rings can cause complications by exciting fluorophores away from the central beam. The effect of out-of-focus excitation can be mitigated by using either a structured illumination approach or by two photon excitation (Planchon et al., 2011). With either approach, isotropic resolution of ~300 nm can be achieved with single-plane frame rates as high as 200 frames per second. The authors demonstrate the usefulness of the technique by imaging the dynamics of several cellular components

including mitochondria, microtubules, filopodia and membrane ruffles (Fig. 2C). The primary advantages of plane illumination microscopy are the reduced photobleaching and the rapid acquisition, making it possible to perform extended live-cell imaging of dynamic processes.

Single-molecule-localization-based super-resolution

In SML-SR, the position of individual fluorophores is found with a precision that can be much higher than the diffraction limit. In practice, this is accomplished by only 'turning on' a small number of fluorophores at a time so that they are isolated from each other, ensuring that their localization can be determined precisely. Stochastic conversion from a dark state to a fluorescent state allows switching on and off of a different sub-set of fluorophores in each image. Repeating this procedure many times allows a super-resolution image to be constructed. Stochastic activation can be achieved through various methods, including photoactivation (Betzig et al., 2006; Hess et al., 2006), photo-switching (Rust et al., 2006; Heilemann et al., 2008) and blinking (Lidke et al., 2005; Lagerholm et al., 2006; Fölling et al., 2008; Dertinger et al., 2009). When a fluorophore is in focus, the x and y positions can be found with good precision. However, because the shape of the emission pattern changes very little when near the focus, z-position estimates have low precision (Ober et al., 2004; Chao et al., 2009). Three approaches have been used to improve 3D localization. In the first approach, additional optics are positioned in the emission path to encode the z-position within the 2D emission pattern, such as inserting a cylindrical lens in the emission path (astigmatic approach) (Huang et al., 2008a) or using a more sophisticated phase modification to generate a 'double-helix' point spread function (Pavani et al., 2009). The second approach is to split the emission into two paths using either a lens, differing optical path lengths or a second objective with the result that two sample planes are imaged simultaneously (Juette et al., 2008; Ram et al., 2009). In the third method, two opposing objectives are positioned to have the same focal plane in the sample and the emission is combined as in an interferometer (Shtengel et al., 2009; Aquino et al., 2011).

The first demonstrations of 3D localization microscopy used total internal reflection (TIR) or near TIR excitation in order to reduce out-of-plane background and were confined to imaging to within ~1 μm from the coverslip. Several groups have now demonstrated the use of 3D SML-SR throughout an entire cell. As noted above, Huang et al. used the addition of a cylindrical lens to encode the z-position of fluorophores in the 2D image (Huang et al., 2008b) (Fig. 2D). When using an oil objective of high numerical aperture to image into water-based samples, chromatic aberrations occur owing to index of refraction mismatch. To reduce these aberrations, Huang et al. immersed their samples in a buffer containing glycerol, which has an index of refraction similar to the immersion oil. The authors used the technique for multi-color immunofluorescence labeling of tubulin and the mitochondria membrane. Multi-color imaging was performed using covalently linked dye pairs that consist of an 'activator' and 'reporter', such that emission of each pair could be independently switched on by its specific activation wavelength. They achieved a lateral localization precision of ~25 nm and an axial precision of ~70 nm (Huang et al., 2008b), revealing contacts between mitochondria and microtubules that could not be resolved with confocal microscopy (Fig. 2D).

Because of the reduced photon yield of photoactivatable fluorescent proteins (PA-FPs) compared with that of organic dye molecules, imaging single PA-FPs results in lower localization precision. The presence of high background fluorescence caused by out-of-focus molecules can lead to an imprecise localization that is unacceptable. York et al. have shown that by confining the photoactivation to the imaged focal plane using two-photon activation, whole cell 3D imaging can be performed with PA-FPs, with the axial position being encoded in the 2D images using the astigmatic approach (York et al., 2011). With this method, they were able to generate images of PA-mCherry-labeled mitochondria with ~50-nm lateral and ~100-nm axial resolution (York et al., 2011).

Interferometric approaches using two opposing objectives to increase the lens aperture have the potential to greatly enhance the precision of the axial localization. The first demonstration of this approach resulted in axial localization precisions of ~10 nm when PA-FPs were used (Shtengel et al., 2009), but was limited to the imaging of a volume of less than 300 nm above the coverslip. Aquino et al. have shown that another approach of coherent collection of light from opposing objectives can be used to localize molecules near a focal plane that is positioned anywhere within a 3D volume of a cell (Aquino et al., 2011). With this set-up, two-color immunofluorescence was used to simultaneously visualize peroxysomes and microtubules with ~10-nm precision in three dimensions.

One clear advantage of SML-SR is that the optical set-ups are relatively simple. In addition, analysis routines continue to be improved and made available to the research community. SML-SR is highly dependent on the photostability, brightness and switching properties of the fluorophores. Fortunately, the popularity of this technique has lead to an increase in the number of fluorophores that have been found to work or are being specifically developed for this technique.

Stimulated emission depletion

STED employs a focused beam of one wavelength to excite fluorophores to the excited singlet state, and a second longer wavelength beam to inhibit fluorescence through stimulated emission in a region surrounding, but excluding the center of, the excitation beam (Fig. 2E) (Hell and Wichmann, 1994). Because of the extreme intensity of light required for stimulated emission, STED is implemented as a point-scanning technique, where the excitation is a single focal spot and the depletion beam is doughnut shaped (Fig. 2E). This results in effective point spread function (PSF) with a size that decreases as the depletion beam intensity increases. In the most common implementation of this approach, resolution of ~30–80 nm is achieved but only in the lateral dimensions. Opazo et al. used STED to image primary hippocampal cell with ~90-nm lateral resolution, but they had to slice their samples into 90-nm thin sections to improve axial resolution (Opazo et al., 2010). The study used two-color immunofluorescence to study the mixing of synaptic vesicles after stimulation and it was observed that vesicle components do not mix (Opazo et al., 2010).

Achieving super-resolution with STED in both lateral and axial dimensions is possible with two approaches. In one approach, the doughnut-shaped depletion beam in the focal plane is supplemented by a second beam that depletes fluorescence above and below the focal plane (Klar et al., 2000; Harke et al., 2008). Wildanger et al. used this approach to image

neurofilaments with lateral and axial resolutions of ~50 nm and ~100 nm, respectively (Wildanger et al., 2009) (Fig. 2E). In another approach, termed isoSTED, Schmidt et al. use two opposing objectives coherently to create depletion beams for both the lateral and axial directions, yielding a 50-nm isotropic resolution of immunolabeled mitochondria (Schmidt et al., 2009). Here, two-color imaging was made possible by alternatively exciting two dyes with different wavelengths of light while using the same STED wavelength.

It is possible to use other physical mechanisms to implement targeted switching of fluorescent molecules to a non-fluorescent state in order to achieve resolution improvement. For example, some fluorescent proteins can be reversibly switched between a dark and fluorescent state using different

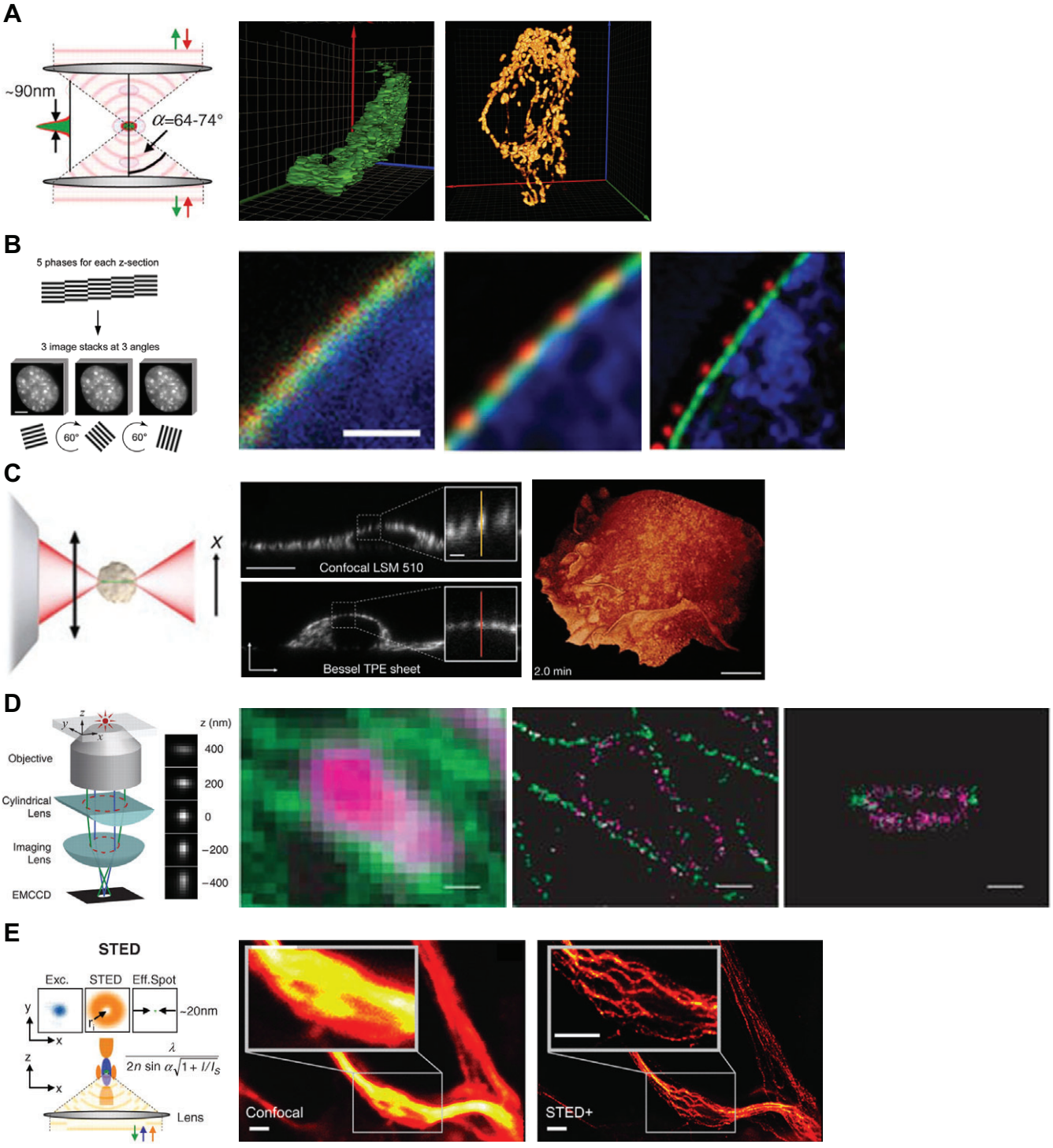

Fig. 2. See next page for legend.

wavelengths of light (Grotjohann et al., 2011). A generalization of techniques, making it possible to perform spatially targeted switching, is called reversible saturable optical fluorescence transitions (RESOLFT) (Hofmann et al., 2005). Targeted switching using photo-convertible probes has the resolution potential of STED but with greatly reduced demands on excitation intensity (Hell, 2007; Grotjohann et al., 2011).

Correlative light and electron microscopy

The fluorescence techniques described above provide extraordinary images of cellular structures; however, only the fluorescently labeled proteins are visualized. So, although fluorescence microscopy provides excellent molecular specificity, it lacks information about the surrounding structures that can be visualized by EM. CLEM combines the advantages of these two techniques to allow direct examination of fluorescence localization within the high-resolution landscape of EM images. Recent advances in probe development, sample preparation and instrumentation are making CLEM more widely accessible (Darcy et al., 2006; Agronskaia et al., 2008; Cortese et al., 2009; Plitzko et al., 2009; Briegel et al., 2010; Bos et al., 2011; Bushby et al., 2011).

Studies from the group of Mark Ellisman have shown that quantum dots (Giepmans et al., 2005) and ReAsH (resorufin arsenical hairpin-binding reagent) (Gaietta et al., 2002) are useful probes for CLEM. Quantum dots have the added advantage that the spectrally distinct labels used for multicolor imaging can also be distinguished by their size and shape at the EM level. However, these probes also have limitations; the large size of the quantum dots can reduce their accessibility to the target, whereas non-specific labeling and harsh treatments required for the use of ReAsH make it less attractive as a probe for cellular structures. Recently, Shu et al. have described a genetically encoded fluorescent protein they call miniSOG, which is an efficient singlet oxygen generator (SOG) that can efficiently photoconvert diaminobenzidine (DAB) for labeling in EM (Box 1) (Shu et al., 2011). The authors demonstrate its use in correlative imaging with markers of the nucleus and mitochondria. Compared with immunogold labeling of connexin at gap junctions, they show that the small miniSOG tag achieves a higher labeling efficiency (Shu et al., 2011) and, therefore, provides a more accurate image.

The group of John Briggs has described the use of fiducial beads for highly accurate correlation between fluorescence microscopy and EM images (Kukulski et al., 2011). They have also demonstrated methods of sample preparation that preserves fluorescence protein integrity in cryofixed samples. With these improvements, they were able to locate GFP- or RFP-tagged proteins by fluorescence and then localize the position of the proteins in the electron micrograph with an accuracy of 100 nm or greater. In addition, they performed EM tomography of the 300-nm section, providing a 3D image of the structures around the fluorescent molecule location (Fig. 3A–D). The authors were able to identify HIV particles binding to the cell surface, image microtubule structure and identify proteins at endocytic sites (Kukulski et al., 2011).

Whereas CLEM is typically performed on fixed samples, van Rijnsoever and colleagues have developed a special cell mounting technique that performs live-cell imaging with fluorescence microscopy first, before the imaged cells are recovered for cryosectioning, immunolabeling and EM imaging (van Rijnsoever et al., 2008). In the first demonstration of this method, they monitored the dynamics of specific endosomes by tracking the lysosomal protein LAMP1 (through a GFP tag). Then, immuno-EM was performed to confirm the LAMP1 content of the tracked endosomes by anti-GFP antibody labeling (van Rijnsoever et al., 2008). Although this work is only a proof-of-principle demonstration, it shows that ‘live-cell CLEM’ has the potential to integrate dynamic information with high-resolution structural information.

Even with standard fluorescence imaging, CLEM allows for identification of proteins in cellular organelles. By integrating super-resolution fluorescence imaging techniques into CLEM, proteins can be localized to organelle substructures with less ambiguity. In the first demonstration of photoactivatable localization microscopy (PALM), Betzig et al. describe the use of photoactivatable proteins to generate an image of the Golgi at sub-diffraction resolution (Betzig et al., 2006). The authors confirmed the improved resolution of PALM by showing that the fluorescence images of the Golgi superimposed within the borders of the Golgi structures in the EM image. This result also demonstrated that localization of fluorescently tagged

Fig. 2. Demonstration of several techniques that produce images with resolution better than the confocal microscope. (**A**) 4pi microscopy uses two opposing lenses focused at the same plane to effectively increase the lens aperture, resulting in improved axial resolution (left) From Hell, 2007. Reprinted with permission from AAAS. The ~100-nm axial resolution of 4pi microscopy (right) reveals mitochondrial fragmentation that was not apparent in confocal microscopy images (center) (Dlasková et al., 2010). Note the lower resolution in the axial dimension (blue axis) as compared to the lateral dimensions. Images reprinted from Dlasková et al., 2010 with permission from Elsevier. (**B**) In SIM, a series of images are collected while scanning the illumination pattern across the sample (left) and are used to reconstruct an image with a lateral resolution improved by about a factor of two compared to confocal microscopy. The three images to the right show 3D SIM images of nuclear pore complex epitopes (red) with respect to the nuclear lamina (green). A nuclear stain (blue) is used as a reference. The resolution achieved was 100 nm and 300 nm in the lateral and axial directions, respectively. Single planes of 3D data sets are compared. The confocal image is on the left, the confocal plus mathematical reconstruction image is in the center and the 3D SIM on the right. From Schermelleh et al., 2008. Reprinted with permission from AAAS. (**C**) A thin ‘Bessel’ beam is swept through the sample while it is maintained in the focal plane of a second imaging objective (left). The resulting 300-nm isotropic resolution is combined with faster imaging speeds (50 two-dimensional frames per second) and dramatically reduced photo-bleaching as compared with that achieved with confocal imaging. Comparison of confocal microscopy (top center) and Bessel beam imaging (bottom center) that used two-photon excitation. The right panel shows one 3D frame of a 73-frame image series. Scale bar: 10 µm. (Planchon et al., 2011). Images reprinted by permission from Macmillan Publishers Ltd: *Nat. Methods* (Planchon et al., 2011), copyright 2011. (**D**) 3D SML-SR of microtubules (green) and mitochondria membrane (magenta). Localization precision was 30 nm laterally and 70 nm axially. Single planes of 3D data sets are shown. The diagram on the left demonstrates how the cylindrical lens encodes the *z*-position in the single molecule image (left). The three images on the right show comparisons between conventional wide field image (left), super-resolution *x*-*y* horizontal section (center), and super-resolution *x*-*y* vertical section (right) are shown. Scale bars are 500 nm. From Huang et al, 2008a. Reprinted with permission from AAAS. (**E**) The STED beam (orange) inhibits fluorescence outside of the center of the focal spot (left). From Hell, 2007. Reprinted with permission from AAAS. The right two images show 3D STED with 50-nm lateral and 100-nm axial resolution images of neurofilaments. The confocal image is in the center and 3D STED image on the right. Images reprinted with permission from Wildanger et al., 2009. Scale bar: 1 µm.

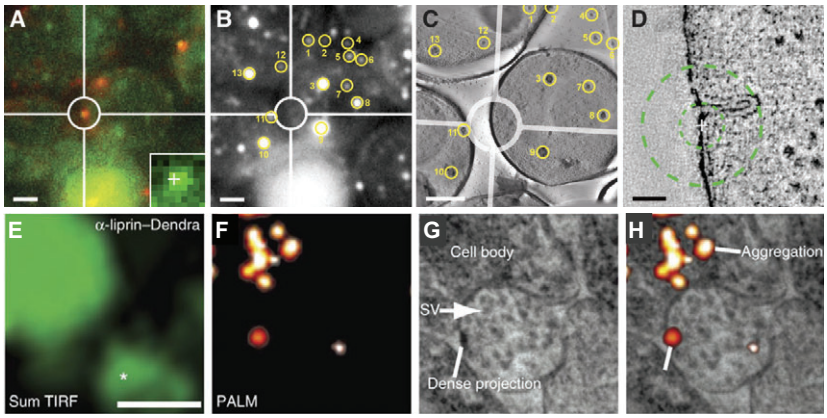

Fig. 3. CLEM allows for localization of proteins to subcellular structures. (**A–D**) Localization of GFP-tagged Rvs167 to endocytic invagination. (A) Wide-field image of Rsv167–EGFP and Abp1–mCherry expressed in *S. cerevisiae*. Inset: GFP signal used for localization of the molecule (cross marks). (B) Image of the fiducial beads used for image correlation. (C) Corresponding fiducial markers in the EM tomograph. (D) High-resolution EM image taken from the tomographic reconstruction that reveals the presence of an endocytic invagination near the location of the Rvs167–GFP. Localization probability of 50% is designated by the inner dashed circle (33 nm) and outer circle of 80% (89 nm). (**E–H**) The improved resolution of PALM reveals the localization of α-liprin–tdEOS to the presynaptic dense projection. (E) Sum TIRF image of α-liprin–tdEOS, representing the typical resolution of the light microscope. (F) PALM image. (G) EM image. (H) Overlay of PALM and EM image. Scale bars: 1 μm (A–C), 50 nm (D), 500 nm (E). Images A–D reproduced from Kukulski et al. (Kukulski et al., 2011). Images E–H reprinted by permission from Macmillan Publishers Ltd: *Nat. Methods* (Watanabe et al., 2011), copyright 2011.

molecules can provide a higher efficiency alternative to immunogold labeling. Recently, Watanabe et al. have compared the use of STED and PALM in CLEM of *C. elegans* (Fig. 3E–H). The authors also compared various fixation methods for optimizing morphology while minimizing autofluorescence and fluorophore quenching, as well as different embedding resins (Watanabe et al., 2011).

Although CLEM is useful for both rapid sample scanning and improved protein localization to organelle structures, routine use of this technique is hampered by the complexity of sample preparation and data acquisition. The introduction of commercial CLEM instruments that facilitate image collection and processing (e.g. Zeiss Shuttle and Find) and the development of integrated fluorescence microscopy and TEM microscopes (Agronskaia et al., 2008) will make this technique more accessible to the non-expert.

Conclusions and perspectives

In this Commentary, we have described techniques for 3D imaging of whole cells that allow the visualization of cellular structures that are crucial to cell function. Tomography technology, including serial section EMT and FIB-SEM, continues to improve and add to our understanding of cellular structure. The recent advances in fluorescence microscopy are providing new ways to generate 3D images of cellular structure with detail finer than the conventional confocal microscope. The integration of EM and fluorescence microscopy in CLEM has created new opportunities to understand protein localization with respect to the surrounding structure. CLEM not only provides a higher density labeling alternative to immuno-gold labeling but also has the potential to localize fluorescent molecule within the 3D structures of an EM tomogram. Together, these technologies will provide new insights into how molecular composition is related to cellular structure.

This is an exciting time for those studying cellular biology. Many of these fluorescence and EM techniques can now be performed using commercial instruments, giving several choices for a technology, particularly for fluorescence imaging. SIM is limited by diffraction to ~100-nm lateral and ~300-nm axial resolution (depending on the emission wavelength) but can be easily used with typical immunofluorescence labeling protocols and dyes. Planar illumination microscopy fills the need for fast and/or extended time-series imaging but only gives limited axial resolution improvement over confocal microscopy. The SML-SR techniques and the STED or RESOLFT techniques truly break the diffraction barrier but the resolution achievable in practice for these techniques is limited by various properties of the fluorophores and, in the case of STED, the intensity of the depletion beam. Continuing development of new probes will make these techniques more robust and accessible, and lead to greater multi-color and live-cell imaging capabilities. In the coming years, these techniques are likely to become standard practice, but as these new tools become more mainstream, interdisciplinary collaborations between technologists and biologists will be needed to give the specialized knowledge often required to accurately use these technological tools, as well as to interpret the results. Ultimately, the integration of information obtained from complementary techniques, such as microscopy, biochemistry and biophysics, will provide the most complete picture of cellular function. The most exciting discoveries are likely to come to those who take full advantage of the capabilities of these emerging technologies.

Funding

The work of our laboratories is supported by a National Science Foundation CAREER Award [grant number MCB-0845062] to D.S.L.; a National Science Foundation CAREER Award [grant number #0954836] to K.A.L.; and the UNM Spatiotemporal Modeling Center, National Institutes of Heath [grant number P50GM085273]. Deposited in PMC for release after 12 months.

References

Agronskaia, A. V., Valentijn, J. A., van Driel, L. F., Schneijdenberg, C. T., Humbel, B. M., van Bergen en Henegouwen, P. M., Verkleij, A. J., Koster, A. J. and Gerritsen, H. C. (2008). Integrated fluorescence and transmission electron microscopy. *J. Struct. Biol.* **164**, 183-189.

Aquino, D., Schönle, A., Geisler, C., Middendorff, C. V., Wurm, C. A., Okamura, Y., Lang, T., Hell, S. W. and Egner, A. (2011). Two-color nanoscopy of three-dimensional volumes by 4Pi detection of stochastically switched fluorophores. *Nat. Methods* **8**, 353-359.

Betzig, E., Patterson, G. H., Sougrat, R., Lindwasser, O. W., Olenych, S., Bonifacino, J. S., Davidson, M. W., Lippincott-Schwartz, J. and Hess, H. F. (2006). Imaging intracellular fluorescent proteins at nanometer resolution. *Science* **313**, 1642-1645.

Bewersdorf, J., Bennett, B. T. and Knight, K. L. (2006). H2AX chromatin structures and their response to DNA damage revealed by 4Pi microscopy. *Proc. Natl. Acad. Sci. USA* **103**, 18137-18142.

Bos, E., SantAnna, C., Gnaegi, H., Pinto, R. F., Ravelli, R. B., Koster, A. J., de Souza, W. and Peters, P. J. (2011). A new approach to improve the quality of ultrathin cryo-sections; its use for immunogold EM and correlative electron cryo-tomography. *J. Struct. Biol.* **175**, 62-72.

Briegel, A., Chen, S., Koster, A. J., Plitzko, J. M., Schwartz, C. L. and Jensen, G. J. (2010). Correlated light and electron cryo-microscopy. *Methods Enzymol.* **481**, 317-341.

Bushby, A. J., P'ng, K. M., Young, R. D., Pinali, C., Knupp, C. and Quantock, A. J. (2011). Imaging three-dimensional tissue architectures by focused ion beam scanning electron microscopy. *Nat. Protoc.* **6**, 845-858.

Chandler, R. J., Zerfas, P. M., Shanske, S., Sloan, J., Hoffmann, V., DiMauro, S. and Venditti, C. P. (2009). Mitochondrial dysfunction in mut methylmalonic acidemia. *FASEB J.* **23**, 1252-1261.

Chao, J., Ram, S., Ward, E. S. and Ober, R. J. (2009). A comparative study of high resolution microscopy imaging modalities using a three-dimensional resolution measure. *Opt. Express* **17**, 24377-24402.

Chen, X., Winters, C. A. and Reese, T. S. (2008). Life inside a thin section: tomography. *J. Neurosci.* **28**, 9321-9327.

Cortese, K., Diaspro, A. and Tacchetti, C. (2009). Advanced correlative light/electron microscopy: current methods and new developments using Tokuyasu cryosections. *J. Histochem. Cytochem.* **57**, 1103-1112.

Darcy, K. J., Staras, K., Collinson, L. M. and Goda, Y. (2006). An ultrastructural readout of fluorescence recovery after photobleaching using correlative light and electron microscopy. *Nat. Protoc.* **1**, 988-994.

Dempsey, G. T., Bates, M., Kowtoniuk, W. E., Liu, D. R., Tsien, R. Y. and Zhuang, X. (2009). Photoswitching mechanism of cyanine dyes. *J. Am. Chem. Soc.* **131**, 18192-18193.

Dertinger, T., Colyer, R., Iyer, G., Weiss, S. and Enderlein, J. (2009). Fast, background-free, 3D super-resolution optical fluctuation imaging (SOFI). *Proc. Natl. Acad. Sci. USA* **106**, 22287-22292.

Dlasková, A., Spacek, T., Santorová, J., Plecitá-Hlavatá, L., Berková, Z., Saudek, F., Lessard, M., Bewersdorf, J. and Jezek, P. (2010). 4Pi microscopy reveals an impaired three-dimensional mitochondrial network of pancreatic islet beta-cells, an experimental model of type-2 diabetes. *Biochim. Biophys. Acta* **1797**, 1327-1341.

Fölling, J., Bossi, M., Bock, H., Medda, R., Wurm, C. A., Hein, B., Jakobs, S., Eggeling, C. and Hell, S. W. (2008). Fluorescence nanoscopy by ground-state depletion and single-molecule return. *Nat. Methods* **5**, 943-945.

Gaietta, G., Deerinck, T. J., Adams, S. R., Bouwer, J., Tour, O., Laird, D. W., Sosinsky, G. E., Tsien, R. Y. and Ellisman, M. H. (2002). Multicolor and electron microscopic imaging of connexin trafficking. *Science* **296**, 503-507.

Galbraith, C. G. and Galbraith, J. A. (2011). Super-resolution microscopy at a glance. *J. Cell Sci.* **124**, 1607-1611.

Giepmans, B. N., Deerinck, T. J., Smarr, B. L., Jones, Y. Z. and Ellisman, M. H. (2005). Correlated light and electron microscopic imaging of multiple endogenous proteins using Quantum dots. *Nat. Methods* **2**, 743-749.

Grotjohann, T., Testa, I., Leutenegger, M., Bock, H., Urban, N. T., Lavoie-Cardinal, F., Willig, K. I., Eggeling, C., Jakobs, S. and Hell, S. W. (2011). Diffraction-unlimited all-optical imaging and writing with a photochromic GFP. *Nature* **478**, 204-208.

Gustafsson, M. G., Shao, L., Carlton, P. M., Wang, C. J., Golubovskaya, I. N., Cande, W. Z., Agard, D. A. and Sedat, J. W. (2008). Three-dimensional resolution doubling in wide-field fluorescence microscopy by structured illumination. *Biophys. J.* **94**, 4957-4970.

Harke, B., Ullal, C. K., Keller, J. and Hell, S. W. (2008). Three-dimensional nanoscopy of colloidal crystals. *Nano Lett.* **8**, 1309-1313.

Heilemann, M., van de Linde, S., Schüttpelz, M., Kasper, R., Seefeldt, B., Mukherjee, A., Tinnefeld, P. and Sauer, M. (2008). Subdiffraction-resolution fluorescence imaging with conventional fluorescent probes. *Angew. Chem. Int. Ed. Engl.* **47**, 6172-6176.

Hell, S. and Stelzer, E. H. K. (1992). Fundamental improvement of resolution with a 4Pi-confocal fluorescence microscope using two-photon excitation. *Opt. Commun.* **93**, 277-282.

Hell, S. W. (2007). Far-field optical nanoscopy. *Science* **316**, 1153-1158.

Hell, S. W. and Wichmann, J. (1994). Breaking the diffraction resolution limit by stimulated emission: stimulated-emission-depletion fluorescence microscopy. *Opt. Lett.* **19**, 780-782.

Hess, S. T., Girirajan, T. P. and Mason, M. D. (2006). Ultra-high resolution imaging by fluorescence photoactivation localization microscopy. *Biophys. J.* **91**, 4258-4272.

Heymann, J. A., Shi, D., Kim, S., Bliss, D., Milne, J. L. and Subramaniam, S. (2009). 3D imaging of mammalian cells with ion-abrasion scanning electron microscopy. *J. Struct. Biol.* **166**, 1-7.

Hofmann, M., Eggeling, C., Jakobs, S. and Hell, S. W. (2005). Breaking the diffraction barrier in fluorescence microscopy at low light intensities by using reversibly photoswitchable proteins. *Proc. Natl. Acad. Sci. USA* **102**, 17565-17569.

Huang, B., Wang, W., Bates, M. and Zhuang, X. (2008a). Three-dimensional super-resolution imaging by stochastic optical reconstruction microscopy. *Science* **319**, 810-813.

Huang, B., Jones, S. A., Brandenburg, B. and Zhuang, X. (2008b). Whole-cell 3D STORM reveals interactions between cellular structures with nanometer-scale resolution. *Nat. Methods* **5**, 1047-1052.

Huang, B., Bates, M. and Zhuang, X. (2009). Super-resolution fluorescence microscopy. *Annu. Rev. Biochem.* **78**, 993-1016.

Huisken, J. and Stainier, D. Y. (2009). Selective plane illumination microscopy techniques in developmental biology. *Development* **136**, 1963-1975.

Jacquier, V., Prummer, M., Segura, J. M., Pick, H. and Vogel, H. (2006). Visualizing odorant receptor trafficking in living cells down to the single-molecule level. *Proc. Natl. Acad. Sci. USA* **103**, 14325-14330.

Juette, M. F., Gould, T. J., Lessard, M. D., Mlodzianoski, M. J., Nagpure, B. S., Bennett, B. T., Hess, S. T. and Bewersdorf, J. (2008). Three-dimensional sub-100 nm resolution fluorescence microscopy of thick samples. *Nat. Methods* **5**, 527-529.

Keller, P. J., Schmidt, A. D., Wittbrodt, J. and Stelzer, E. H. K. (2008). Reconstruction of zebrafish early embryonic development by scanned light sheet microscopy. *Science* **322**, 1065-1069.

Klar, T. A., Jakobs, S., Dyba, M., Egner, A. and Hell, S. W. (2000). Fluorescence microscopy with diffraction resolution barrier broken by stimulated emission. *Proc. Natl. Acad. Sci. USA* **97**, 8206-8210.

Koster, A. J. and Klumperman, J. (2003). Electron microscopy in cell biology: integrating structure and function. *Nat. Rev. Mol. Cell Biol.* **Suppl.** SS6-SS10.

Kukulski, W., Schorb, M., Welsch, S., Picco, A., Kaksonen, M. and Briggs, J. A. (2011). Correlated fluorescence and 3D electron microscopy with high sensitivity and spatial precision. *J. Cell Biol.* **192**, 111-119.

Lagerholm, B. C., Averett, L., Weinreb, G. E., Jacobson, K. and Thompson, N. L. (2006). Analysis method for measuring submicroscopic distances with blinking quantum dots. *Biophys. J.* **91**, 3050-3060.

Lešer, V., Drobne, D., Pipan, Z., Milani, M. and Tatti, F. (2009). Comparison of different preparation methods of biological samples for FIB milling and SEM investigation. *J. Microsc.* **233**, 309-319.

Lidke, K., Rieger, B., Jovin, T. and Heintzmann, R. (2005). Superresolution by localization of quantum dots using blinking statistics. *Opt. Express* **13**, 7052-7062.

Mannella, C. A., Marko, M., Penczek, P., Barnard, D. and Frank, J. (1994). The internal compartmentation of rat-liver mitochondria: tomographic study using the high-voltage transmission electron microscope. *Microsc. Res. Tech.* **27**, 278-283.

Mannella, C. A., Marko, M. and Buttle, K. (1997). Reconsidering mitochondrial structure: new views of an old organelle. *Trends Biochem. Sci.* **22**, 37-38.

Mazel, T., Raymond, R., Raymond-Stintz, M., Jett, S. and Wilson, B. S. (2009). Stochastic modeling of calcium in 3D geometry. *Biophys. J.* **96**, 1691-1706.

Murk, J. L., Lebbink, M. N., Humbel, B. M., Geerts, W. J., Griffith, J. M., Langenberg, D. M., Verreck, F. A., Verkleij, A. J., Koster, A. J., Geuze, H. J. et al. (2004). 3-D Structure of multilaminar lysosomes in antigen presenting cells reveals trapping of MHC II on the internal membranes. *Traffic* **5**, 936-945.

Murphy, G. E., Lowekamp, B. C., Zerfas, P. M., Chandler, R. J., Narasimha, R., Venditti, C. P. and Subramaniam, S. (2010). Ion-abrasion scanning electron microscopy reveals distorted liver mitochondrial morphology in murine methylmalonic acidemia. *J. Struct. Biol.* **171**, 125-132.

Noske, A. B., Costin, A. J., Morgan, G. P. and Marsh, B. J. (2008). Expedited approaches to whole cell electron tomography and organelle mark-up in situ in high-pressure frozen pancreatic islets. *J. Struct. Biol.* **161**, 298-313.

Ober, R. J., Ram, S. and Ward, E. S. (2004). Localization accuracy in single-molecule microscopy. *Biophys. J.* **86**, 1185-1200.

Opazo, F., Punge, A., Bückers, J., Hoopmann, P., Kastrup, L., Hell, S. W. and Rizzoli, S. O. (2010). Limited intermixing of synaptic vesicle components upon vesicle recycling. *Traffic* **11**, 800-812.

Palade, G. E. (1952). The fine structure of mitochondria. *Anat. Rec.* **114**, 427-451.

Patterson, G., Davidson, M., Manley, S. and Lippincott-Schwartz, J. (2010). Superresolution imaging using single-molecule localization. *Annu. Rev. Phys. Chem.* **61**, 345-367.

Pavani, S. R., Thompson, M. A., Biteen, J. S., Lord, S. J., Liu, N., Twieg, R. J., Piestun, R. and Moerner, W. E. (2009). Three-dimensional, single-molecule fluorescence imaging beyond the diffraction limit by using a double-helix point spread function. *Proc. Natl. Acad. Sci. USA* **106**, 2995-2999.

Planchon, T. A., Gao, L., Milkie, D. E., Davidson, M. W., Galbraith, J. A., Galbraith, C. G. and Betzig, E. (2011). Rapid three-dimensional isotropic imaging of living cells using Bessel beam plane illumination. *Nat. Methods* **8**, 417-423.

Plitzko, J. M., Rigort, A. and Leis, A. (2009). Correlative cryo-light microscopy and cryo-electron tomography: from cellular territories to molecular landscapes. *Curr. Opin. Biotechnol.* **20**, 83-89.

Porter, K. R., Claude, A. and Fullam, E. F. (1945). A study of tissue culture cells by electron microscopy: methods and preliminary observations. *J. Exp. Med.* **81**, 233-246.

Ram, S., Prabhat, P., Ward, E. S. and Ober, R. J. (2009). Improved single particle localization accuracy with dual objective multifocal plane microscopy. *Opt. Express* **17**, 6881-6898.

Regoes, A. and Hehl, A. B. (2005). SNAP-tag mediated live cell labeling as an alternative to GFP in anaerobic organisms. *Biotechniques* **39**, 809-812.

Journal of Cell Science

Rizzuto, R., Pinton, P., Carrington, W., Fay, F. S., Fogarty, K. E., Lifshitz, L. M., Tuft, R. A. and Pozzan, T. (1998). Close contacts with the endoplasmic reticulum as determinants of mitochondrial Ca2+ responses. *Science* **280**, 1763-1766.

Rust, M. J., Bates, M. and Zhuang, X. (2006). Sub-diffraction-limit imaging by stochastic optical reconstruction microscopy (STORM). *Nat. Methods* **3**, 793-796.

Schermelleh, L., Carlton, P. M., Haase, S., Shao, L., Winoto, L., Kner, P., Burke, B., Cardoso, M. C., Agard, D. A., Gustafsson, M. G. et al. (2008). Subdiffraction multicolor imaging of the nuclear periphery with 3D structured illumination microscopy. *Science* **320**, 1332-1336.

Schermelleh, L., Heintzmann, R. and Leonhardt, H. (2010). A guide to super-resolution fluorescence microscopy. *J. Cell Biol.* **190**, 165-175.

Schmidt, R., Wurm, C. A., Punge, A., Egner, A., Jakobs, S. and Hell, S. W. (2009). Mitochondrial cristae revealed with focused light. *Nano Lett.* **9**, 2508-2510.

Shao, L., Isaac, B., Uzawa, S., Agard, D. A., Sedat, J. W. and Gustafsson, M. G. (2008). I5S: wide-field light microscopy with 100-nm-scale resolution in three dimensions. *Biophys. J.* **94**, 4971-4983.

Shroff, H., Galbraith, C. G., Galbraith, J. A., White, H., Gillette, J., Olenych, S., Davidson, M. W. and Betzig, E. (2007). Dual-color superresolution imaging of genetically expressed probes within individual adhesion complexes. *Proc. Natl. Acad. Sci. USA* **104**, 20308-20313.

Shtengel, G., Galbraith, J. A., Galbraith, C. G., Lippincott-Schwartz, J., Gillette, J. M., Manley, S., Sougrat, R., Waterman, C. M., Kanchanawong, P., Davidson, M. W. et al. (2009). Interferometric fluorescent super-resolution microscopy resolves 3D cellular ultrastructure. *Proc. Natl. Acad. Sci. USA* **106**, 3125-3130.

Shu, X., Lev-Ram, V., Deerinck, T. J., Qi, Y., Ramko, E. B., Davidson, M. W., Jin, Y., Ellisman, M. H. and Tsien, R. Y. (2011). A genetically encoded tag for correlated light and electron microscopy of intact cells, tissues, and organisms. *PLoS Biol.* **9**, e1001041.

Subach, F. V., Patterson, G. H., Manley, S., Gillette, J. M., Lippincott-Schwartz, J. and Verkhusha, V. V. (2009). Photoactivatable mCherry for high-resolution two-color fluorescence microscopy. *Nat. Methods* **6**, 153-159.

Szent-Gyorgyi, C., Schmidt, B. F., Creeger, Y., Fisher, G. W., Zakel, K. L., Adler, S., Fitzpatrick, J. A., Woolford, C. A., Yan, Q., Vasilev, K. V. et al. (2008). Fluorogen-activating single-chain antibodies for imaging cell surface proteins. *Nat. Biotechnol.* **26**, 235-240.

Toomre, D. and Bewersdorf, J. (2010). A new wave of cellular imaging. *Annu. Rev. Cell Dev. Biol.* **26**, 285-314.

van Rijnsoever, C., Oorschot, V. and Klumperman, J. (2008). Correlative light-electron microscopy (CLEM) combining live-cell imaging and immunolabeling of ultrathin cryosections. *Nat. Methods* **5**, 973-980.

Watanabe, S., Punge, A., Hollopeter, G., Willig, K. I., Hobson, R. J., Davis, M. W., Hell, S. W. and Jorgensen, E. M. (2011). Protein localization in electron micrographs using fluorescence nanoscopy. *Nat. Methods* **8**, 80-84.

West, M., Zurek, N., Hoenger, A. and Voeltz, G. K. (2011). A 3D analysis of yeast ER structure reveals how ER domains are organized by membrane curvature. *J. Cell Biol.* **193**, 333-346.

Wildanger, D., Medda, R., Kastrup, L. and Hell, S. W. (2009). A compact STED microscope providing 3D nanoscale resolution. *J. Microsc.* **236**, 35-43.

Wilson, B. S., Pfeiffer, J. R. and Oliver, J. M. (2000). Observing FcepsilonRI signaling from the inside of the mast cell membrane. *J. Cell Biol.* **149**, 1131-1142.

York, A. G., Ghitani, A., Vaziri, A., Davidson, M. W. and Shroff, H. (2011). Confined activation and subdiffractive localization enables whole-cell PALM with genetically expressed probes. *Nat. Methods* **8**, 327-333.